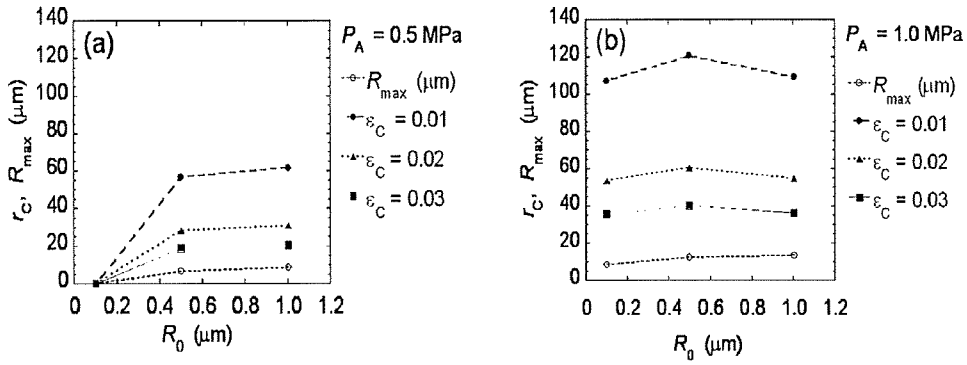

Fig. 6 Potential radius r_C of inducing cell damage by a shock wave from a cavitation bubble and the maximum bubble expansion radius R_{max}, where r_C was given by eqn (4). The initial bubble radius R_0 was 0.1–1.0 μm. The critical strain ε_C was 0.01– 0.03. The US pressure P_A was 0.5–1.0 MPa. The US frequency f was 1 MHz. Numerical data were obtained using a fourth-order Runge-Kutta method.

bubble was calculated to be 19 μm prior to the US exposure. If a single NB produces multiple cavitation bubbles, the conditions $r_C > r_0$ and $r_C > R_{max}$ are satisfied, i.e., the entire area of the medium can be regarded as the shock wave dominant area; therefore, all cells in the medium would be loaded by the shock waves created by the cavitation bubbles.

Figure 7 shows the relationship between P_A and the impulse Ir_c at r_C with varying ε_C, given by eqn (10) at the US frequency f of 1 MHz. When R_0 = 0.5 μm (Fig. 7a), a peak of each characteristic line was obtained at P_A = 0.3 MPa, and the value increased with increasing ε_C. The peak was due to the bubble natural frequency. When R_0 = 1.0 μm (Fig. 7b), peaks were not observed in the figure; however, the lines decreased rapidly with increasing P_A to reach a constant value. This figure indicates that a spherical cavitation bubble with a radius of 0.5–1.0 μm generates impulse values up to 100 mPa·s.

MD simulation of water molecular delivery into the lipid bilayer with shock wave impulse

It is desirable to calculate the number of calcein molecules delivered into cells with MD simulation for comparison with the experimental results. However, to our knowledge, there are no reliable calculation parameters such as force fields or partial charges to reproduce calcein thermodynamic properties and quantum factors. In the present study, we compared the number of water molecules delivered into the lipid bilayer calculated by MD simulation with that of calcein molecules obtained experimentally.

Figure 8 shows the relationship between the shock wave impulse and the penetration rate of water molecules into the bilayer obtained by MD simulation. The penetration ratio of water molecules into the lipid bilayer increased with increasing shock wave impulse. Water molecules were delivered into the cells at the rate of 0–0.3 molecules/(ps·nm^2) at I = 0–11 mPa·s at R_0 = 0.5 μm and ε_C = 0.03 (Figs. 7a and 8). In contrast, at R_0 = 1.0 μm and ε_C = 0.03 (Figs. 7b and 8), water molecules were delivered into the cells at a rate of 0.2–7.6 molecules/(ps·nm^2) at I = 7.2–95 mPa·s.

Although it is reported that water molecules can penetrate into the cytoplasm across the membrane on macroscopic time scales [51], the event rarely occurs on molecular time scales (below nanosecond time scales). However, in the present molecular simulation, water penetration was observed on picosecond time scales. Here, we assumed that at the cell radius r of 5 μm, the shock wave impulse was loaded to a cell from above, and the duration of the impulse was 1 ps. The surface area of the cell hemisphere was given by $2\pi r^2$, and the number of water molecules delivered into the lipid bilayer was calculated to be around 10^7~10^9. The radius of the water molecule was approximately 0.1 nm, and the radius of calcein was estimated to be 0.68 nm [30]. Although the size of the calcein molecule was

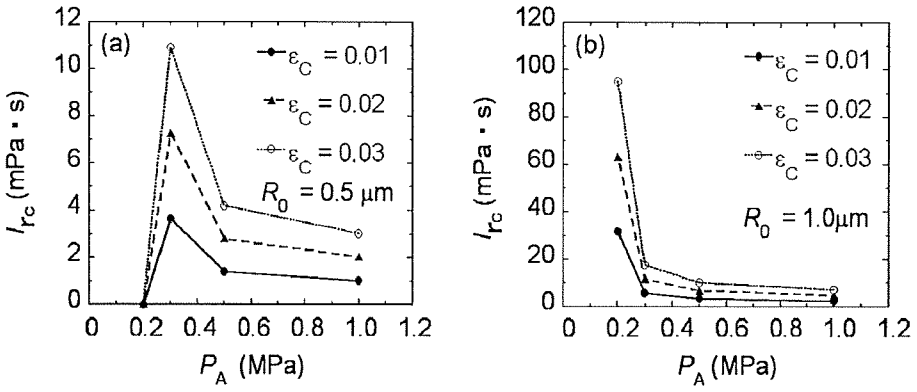

Fig. 7 Relationship between the shock wave impulse Ir_C (mPa·s) and the US pressure P_A (0.2–1.0 MPa). The US frequency f was 1 MHz. The critical strain ε_C was 0.01–0.03. (a) R_0 = 0.5 μm, (b) R_0 = 1.0 μm. Numerical data were obtained using a fourth-order Runge-Kutta method.

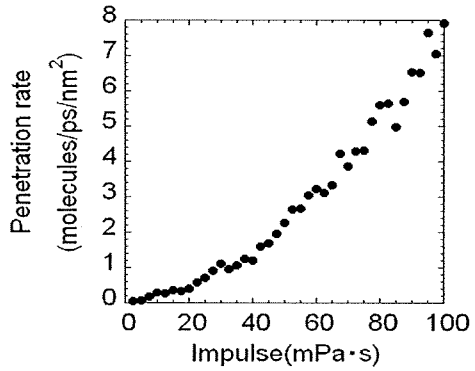

Fig. 8 Relationship between the shock wave impulse and the penetration ratio of water molecules calculated by MD simulation, in which the penetration ratio was calculated in the hydrophobic region at the instant of termination of simulation divided by the cross-sectional area (A = 10.25 nm^2) and the simulation time.

larger than that of the water molecule by a factor of 6.8, the number of delivered calcein molecules in the order of 10^7 per cell (Fig. 3) corresponded to the numerical values. We should note that the estimation of calcein delivery is on experimental time scales (several seconds have elapsed after exposure to ultrasound). On these time scales, the number of delivered water molecules might become considerably larger than that of calcein molecules because many shock waves are generated by pulsating bubbles' impact on membranes. At present, we have investigated water pore formation in lipid bilayers induced by the shock wave impulse [33]. This study suggests that more water penetration induces more larger structural changes in the lipid bilayer. Although it is not possible to estimate the number of water molecules that penetrate into the cells after induction by shock waves by using any other method, the results of the experimental estimation of calcein and numerical estimation of water molecules in the present study imply that the penetration of a large number of water molecules is required before the entry of large molecules. Because water penetration depends on the shock wave impulse generated in the conditions studied here, we believe that the impulse of the shock waves generated by the cavitation bubbles is one of the important parameters for permeabilization during sonoporation.

4. Conclusion

In the present study, experimental, theoretical and numerical analyses were performed to investigate cavitation bubbles mediated molecular delivery during sonoporation. The following conclusions were obtained.

1. Experimental observation using lipid nano/microbubbles indicated that increasing US

pressure increased uptake of fluorescent molecules, calcein, into 293T human, and decreased survival fraction.

2. Theoretical analysis based on a spherical gas bubble dynamics indicated that the impulse of the shock wave (i.e., the pressure integrated over time) generated by the collapse of a cavitation bubble created by nano/microbubbles was one of dominant factors for exogenous molecules to enter into the cell membrane rather than bubble expansion.

3. Molecular dynamics simulation revealed that the number of exogenous molecules delivered into the cell membrane increased with increasing the shock wave impulse.

4. The impulse of the shock wave generated by cavitation bubbles was one of important parameters for causing exogenous molecular uptake into living cells during sonoporation.

Acknowledgments

TK acknowledges the Grant-in-Aid for Scientific Research (B) (20300173); the Grants-in-Aid for Scientific Research on Priority Area, MEXT (20015005); and the Grant for Research on Advanced Medical Technology, the Ministry of Health, Labour and Welfare of Japan (H19-nano-010). YT acknowledges the Grant-in-Aid for Scientific Research (C) (20560144), and KK acknowledges the Grant-in-Aid for Young Scientists (B) (20760114—0004).

Appendix

Atomized liquid particles generated with US

The mean diameter d of the atomized particles due to capillary waves generated by US on the free surface is given by the equation [57]:

$$d \cong 1.9\left[\frac{\sigma_L}{\rho_L f^2}\right]^{\frac{1}{3}} \tag{A1}$$

where f is the acoustic frequency (varied from 20 kHz to 3 MHz); ρ_L, the liquid density (997 kg/m^3 for water at 25°C); and σ_L, the liquid surface tension of 72 mN/m. Thus, the mean diameter of the atomized particles was calculated to be 7.9 μm for 1 MHz US. The detailed mechanism of atomized particle generation has been reported by Yule and Al-Suleimani [52].

Characteristic radius r_0 occupied by a single bubble

In the abovementioned calcein experiment, 110 μL of a medium that contained 10% NBs was irradiated by US. The maximum geometrical characteristic radius r_0 occupied uniformly by a single NB is given as follows:

$$r_0 = \left(\frac{3Ah}{4\pi N_0}\right)^{\frac{1}{3}} \tag{A2}$$

where A is the area of the base of a well in the 48-well plate; h, height of the medium; N_0, the number of US contrast agents. For micelle bubbles, r_0 was calculated to be 19 μm at $N_0 = 3.4 \times 10^8$ bubbles/mL.

References

(1) H. Zhegn, O. Mukdadi, R. Shandas, Theoretical predictions of harmonic generation from submicron ultrasound contrast agents for nonlinear biomedical ultrasound imaging. *Physics in Medicine and Biology*, Vol.51, No.3 (2006), pp.557-573.

(2) W. Hayduk, H. Laudie, Prediction of diffusion-coefficients for nonelectrolytes in dilute

aqueous-solutions. *Aiche Journal*, Vol.20, No.3 (1974), pp.611-615.

(3) A. Kabalnov, D. Klein, T. Pelura, E. Schutt, J. Weers, Dissolution of multicomponent microbubbles in the bloodstream: 1. Theory. *Ultrasound in Medicine and Biology*, Vol.24, No.5 (1998), pp.739-749.

(4) E.C. Unger, T. Porter, W. Culp, R. Labell, T. Matsunaga, R. Zutshi, Therapeutic applications of lipid-coated microbubbles. *Advanced Drug Delivery Reviews*, Vol.56, No.9 (2004), pp.1291-1314.

(5) J.R. Lindner, Microbubbles in medical imaging: current applications and future directions. *Nature Reviews Drug Discovery*, Vol.3, No.6 (2004), pp.527-532.

(6) R. Bekeredjian, S. Chen, P.A. Frenkel, P.A. Grayburn, R.V. Shohet, Ultrasound-targeted microbubble destruction can repeatedly direct highly specific plasmid expression to the heart. *Circulation*, Vol.108, No.8 (2003), pp.1022-1026.

(7) T.R. Porter, P.L. Iversen, S. Li, F. Xie, Interaction of diagnostic ultrasound with synthetic oligonucleotide-labeled perfluorocarbon-exposed sonicated dextrose albumin microbubbles. *Journal of Ultrasound in Medicine*, Vol.15, No.8 (1996), pp.577-584.

(8) S.M. Stieger, C.F. Caskey, R.H. Adamson, S. Qin, F.R. Curry, E.R. Wisner, K.W. Ferrara, Enhancement of vascular permeability with low-frequency contrast-enhanced ultrasound in the chorioallantoic membrane model. *Radiology*, Vol.243, No.1 (2007), pp.112-121.

(9) A.Y. Ammi, R.O. Cleveland, J. Mamou, G.I. Wang, S.L. Bridal, W.D. O'Brien, Ultrasonic contrast agent shell rupture detected by inertial cavitation and rebound signals. *IEEE Transactions on Ultrasonics Ferroelectrics and Frequency Control*, Vol.53, No.1 (2006), pp.126-136.

(10) S.H. Chen, X.H. Chen, Y. Wang, K. Kosai, M.J. Finegold, S.S. Rich, S.L. Woo, Combination gene therapy for liver metastasis of colon carcinoma in vivo. *The Proceedings of the National Academy of Sciences of the United States of America*, Vol.92, No.7 (1995), pp.2577-2581.

(11) P.P. Kamaev, J.D. Hutcheson, M.L. Wilson, M.R. Prausnitz, Quantification of optison bubble size and lifetime during sonication dominant role of secondary cavitation bubbles causing acoustic bioeffects. *Journal of the Acoustical Society of America*, Vol.115, No.4 (2004), pp.1818-1825.

(12) J. Wu, J. Tong, Experimental study of stability of a contrast agent in an ultrasound field. *Ultrasound in Medicine and Biology*, Vol.24, No.2 (1998), pp.257-265.

(13) H.R. Guzman, D.X. Nguyen, S. Khan, M.R. Prausnitz, Ultrasound-mediated disruption of cell membranes. I. Quantification of molecular uptake and cell viability. *Journal of the Acoustical Society of America*, Vol.110, No.1 (2001), pp.588-596.

(14) A. van Wamel, K. Kooiman, M. Harteveld, M. Emmer, F.J. ten Cate, M. Versluis, N. de Jong, Vibrating microbubbles poking individual cells: drug transfer into cells via sonoporation. *Journal of Control Release*, Vol.112, No.2 (2006), pp.149-155.

(15) T. Li, K. Tachibana, M. Kuroki, Gene transfer with echo-enhanced contrast agents: comparison between Albunex, Optison, and Levovist in mice--initial results. *Radiology*, Vol.229, No.2 (2003), pp.423-428.

(16))X. Wang, H.D. Liang, B. Dong, Q.L. Lu, M.J. Blomley, Gene transfer with microbubble ultrasound and plasmid DNA into skeletal muscle of mice: comparison between commercially available microbubble contrast agents. *Radiology*, Vol.237, No.1 (2005), pp.224-229.

(17) H.R. Guzman, A.J. McNamara, D.X. Nguyen, M.R. Prausnitz, Bioeffects caused by changes in acoustic cavitation bubble density and cell concentration: A unified explanation based on cell-to-bubble ratio and blast radius. *Ultrasound in Medicine and Biology*, Vol.29, No.8 (2003), pp.1211-1222.

(18) M. Ward, J. Wu, J.F. Chiu, Experimental study of the effects of Optison concentration on sonoporation in vitro. *Ultrasound in Medicine and Biology*, Vol.26, No.7 (2000),

pp.1169-1175.

(19) E.N. Harvey, D.K. Barnes, W.D. McElroy, A.H. Whiteley, D.C. Pease, K.W. Cooper, Bubble formation in animals. *Journal of cellular and comparative physiology*, Vol.24 (1944), pp.1-22.

(20) R.E. Apfel, C.K. Holland, Gauging the likelihood of cavitation from short-pulse, low-duty cycle diagnostic ultrasound. *Ultrasound in Medicine and Biology*, Vol.17, No.2 (1991), pp.179-185.

(21) W.S. Chen, T.J. Matula, L.A. Crum, The disappearance of ultrasound contrast bubbles: observations of bubble dissolution and cavitation nucleation. *Ultrasound in Medicine and Biology*, Vol.28, No.6 (2002), pp.793-803.

(22) D.L. Miller, R.M. Thomas, Ultrasound contrast agents nucleate inertial cavitation in vitro. *Ultrasound in Medicine and Biology*, Vol.21, No.8 (1995), pp.1059-1065.

(23) D.M. Hallow, A.D. Mahajan, T.E. McCutchen, M.R. Prausnitz, Measurement and correlation of acoustic cavitation with cellular bioeffects. *Ultrasound in Medicine and Biology*, Vol.32, No.7 (2006), pp.1111-1122.

(24) D.M. Skyba, R.J. Price, A.Z. Linka, T.C. Skalak, S. Kaul, Direct in vivo visualization of intravascular destruction of microbubbles by ultrasound and its local effects on tissue. *Circulation*, Vol.98, No.4 (1998), pp.290-293.

(25) M.J. Shortencarier, P.A. Dayton, S.H. Bloch, P.A. Schumann, T.O. Matsunaga, K.W. Ferrara, A method for radiation-force localized drug delivery using gas-filled lipospheres. *IEEE Transactions on Ultrasonics, Ferroelectrics, and Frequency Control*, Vol.51, No.7 (2004), pp.822-831.

(26) T. Kodama, Y. Tomita, K. Koshiyama, M.J. Blomley, Transfection effect of microbubbles on cells in superposed ultrasound waves and behavior of cavitation bubble. *Ultrasound in Medicine and Biology*, Vol.32, No.6 (2006), pp.905-914.

(27) S. Gambihler, M. Delius, J.W. Ellwart, Permeabilization of the plasma-membrane of L1210 mouse leukemia-cells using lithotripter shock-waves. *Journal of Membrane Biology*, Vol.141, No.3 (1994), pp.267-275.

(28) T. Kodama, A.G. Doukas, M.R. Hamblin, Shock wave-mediated molecular delivery into cells. *Biochimica et Biophysica Acta*, Vol.1542, No.13 (2002), pp.186-194.

(29) A.G. Doukas, D.J. McAuliffe, T.J. Flotte, Biological effects of laser-induced shock waves: structural and functional cell damage in vitro. *Ultrasound in Medicine and Biology*, Vol.19, No.2 (1993), pp.137-146.

(30) T. Kodama, M.R. Hamblin, A.G. Doukas, Cytoplasmic molecular delivery with shock waves: importance of impulse. *Biophysical Journal*, Vol.79, No.4 (2000), pp.1821-1832.

(31) K. Koshiyama, T. Kodama, T. Yano, S. Fujikawa, Structural change in lipid bilayers and water penetration induced by shock waves: molecular dynamics simulations. *Biophysical Journal*, Vol.91, No.6 (2006), pp.2198-2205.

(32) K. Koshiyama, T. Kodama, T. Yano, S. Fujikawa, Molecular dynamics simulation of structural changes of lipid bilayers induced by shock waves: Effects of incident angles. *Biochimica et Biophysica Acta*, Vol.1778, No.6 (2008), pp.1423-1428.

(33) K. Koshiyama, T. Kodama, T. Yano, S. Fujikawa, Molecular dynamics simulation of water pore formation in lipid bilayer induced by shock waves. *Therapeutic Ultrasound: 5th International Symposium on Therapeutic Ultrasound*, Vol. 829, (2005), pp.583-587.

(34) A. Aoi, Y. Watanabe, S. Mori, M. Takahashi, G. Vassaux, T. Kodama, Herpes simplex virus thymidine kinase-mediated suicide gene therapy using nano/microbubbles and ultrasound. *Ultrasound in Medicine and Biology*, Vol.34, No.3 (2008), pp.425-434.

(35) J.R. Tennant, Evaluation of the trypan blue technique for determination of cell viability. *Transplantation*, Vol.2 (1964), pp.685-694.

(36))T. Kodama, A.G. Doukas, M.R. Hamblin, Delivery of ribosome-inactivating protein toxin into cancer cells with shock waves. *Cancer Letters*, Vol.189, No.1 (2003), pp.69-75.

(37) M. Postema, A. Bouakaz, M. Versluis, N. de Jong, Ultrasound-induced gas release from contrast agent microbubbles. *IEEE Transactions on Ultrasonics, Ferroelectrics, and Frequency Control*, Vol.52, No.6 (2005), pp.1035-1041.

(38) B. Wolfrum, R. Mettin, T. Kurz, W. Lauterborn, Observations of pressure-wave-excited contrast agent bubbles in the vicinity of cells. *Applied Physics Letters*, Vol.81, No.26 (2002), pp.5060-5062.

(39) C.D. Ohl, M. Arora, R. Ikink, N. de Jong, M. Versluis, M. Delius, D. Lohse, Sonoporation from jetting cavitation bubbles. *Biophysical Journal*, Vol.91, No.11 (2006), pp.4285-4295.

(40) J.R. Blake, B.B. Taib, G. Doherty, Transient cavities near boundaries .1. rigid boundary. *Journal of Fluid Mechanics*, Vol.170 (1986), pp.479-497.

(41) J.R. Blake, B.B. Taib, G. Doherty, Transient cavities near boundaries .2. free-surface. *Journal of Fluid Mechanics*, Vol.181 (1987), pp.197-212.

(42) A. Shima, K. Takayama, Y. Tomita, N. Miura, An experimental study on effects of a solid wall on the motion of bubbles and shock waves in bubble collapse. *Acustica*, Vol.48, No.5 (1981), pp.293-301.

(43) J.B. Keller, M. Miksis, Bubble oscillations of large amplitude. *Journal of the Acoustical Society of America*, Vol.68, No.2 (1980), pp.628-633.

(44) A. Prosperetti, A. Lezzi, Bubble Dynamics in a Compressible Liquid .1. 1st-Order Theory. *Journal of Fluid Mechanics*, Vol.168 (1986), pp.457-478.

(45) P.A. Dayton, J.E. Chomas, A.F.H. Lum, J.S. Allen, J.R. Lindner, S.I. Simon, K.W. Ferrara, Optical and acoustical dynamics of microbubble contrast agents inside neutrophils. *Biophysical Journal*, Vol.80, No.3 (2001), pp.1547-1556.

(46) J. Sundaram, B.R. Mellein, S. Mitragotri, An experimental and theoretical analysis of ultrasound-induced permeabilization of cell membranes. *Biophysical Journal*, Vol.84, No.5 (2003), pp.3087-3101.

(47) E.A. Evans, R. Waugh, L. Melnik, Elastic area compressibility modulus of red cell membrane. *Biophysical Journal*, Vol.16, No.6 (1976), pp.585-595.

(48) R. Hickling, M. Plesset, Collapse and rebound of a spherical bubble in water. *Physics of Fluids*, Vol.7, No.1 (1964), pp.7-14.

(49) R.H. Cole, Underwater Explosions, *Princeton University Press, Princeton, NJ*, (1948).

(50) Y. Tomita, M. Tsubota, N. An-Naka, Energy evaluation of cavitation bubble generation and shock wave emission by laser focusing in liquid nitrogen. *Journal of Applied Physics*, Vol.93, No.5 (2003), pp.3039-3048.

(51) B. Alberts, D. Bray, J. Lewis, M. Raff, K. Roberts, J.D. Watson, *Molecular biology of the cell,* Garland Publishing, Inc., New York & London, (1994).

(52) A.J. Yule, Y. Al-Suleimani, On droplet formation from capillary waves on a vibrating surface. *Proceedings of the Royal Society of London Series a-Mathematical Physical and Engineering Sciences*, Vol.456, No.1997 (2000), pp.1069-1085.

(53) S. Bao, B.D. Thrall, D.L. Miller, Transfection of a reporter plasmid into cultured cells by sonoporation in vitro. *Ultrasound in Medicine and Biology*, Vol.23, No.6 (1997), pp.953-959.

(54) T. Tsujino, A. Shima, The Behavior of Gas-Bubbles in Blood Subjected to an Oscillating Pressure. *Journal of Biomechanics*, Vol.13, No.5 (1980), pp.407-416.

(55) S. Fujikawa, T. Akamatsu, Effects of the non-equilibrium condensation of vapour on the pressure wave produced by the collapse of a bubble in a liquid. *Journal of Fluid Mechanics*, Vol.97, No.3 (1980), pp.481-512.

(56) Y. Tomita, A. Shima, On the behavior of a spherical bubble and the impulse pressure in a viscous compressible liquid. *Bulletin of the JSME*, Vol.20, No.149 (1977), pp.1453-1460.

(57) C. Chiba, Study on atomization of liquid due to ultrasound oscillation. *Ph.D. Thesis, Engineering, Tohoku University, Sendai*, (1983).

2-7. Genetic Analysis of Arsenic Toxicities Using an Experimental Mouse Model

INTRODUCTION

Development of the first organisms on the Earth took place 8 hundred million years after the Earth's birth. Thereafter, organisms have evolved over 8 billion, 8 hundred million years until the present. There are now1.5 million different species on Earth, including 1.2 million species of animals and 0.3 million species of plants. In addition, it is assumed that about 1.5 million species have gone extinct.

Species survival is controlled by natural selection, involving interspecies struggle with the natural environment. The potential for survival exists in germ line mutations of organisms randomly occurring in various species, which arise because the reproduction of DNA for the next generation is not perfect. Mutations occur in a creature group since it is vague, and they accumulate latently and are preserved as genomic polymorphisms in species. Such mutations result in the ability of individuals of a given species to develop phenotypes profitable to changes in their environment at a given point in time, and may thus enable a species to survive or evolve over time. Organisms existing on the Earth at present are only here as a result of the accumulation of such mutations over millions of years.

The Earth's environment now deviates from its "natural" frame. This is now controlled by Homo sapiens, presently at the apex of the ecosystem. Toxic chemicals which damage various organisms play a large role in such an environment, and are thought to induce latent species selection. We still do not completely comprehend the process of species selection. If we can clarify the kinds of germ line mutations preserved in a creature group that become a target of selection by toxic chemicals, this may help us to elucidate various evolutionary mechanisms.

We used an inbred strain of mice in this analysis, whose genomic DNA was homogeneous. We established recombinant inbred (RI) strains of mice using two different parental inbred strains as progenitors, which have mutations on genome DNA different from each other, followed by an F1 intercross and more than 20 generations of strict brother-sister mating (Fig. 1). This breeding protocol allows the production of a family of new inbred strains with special properties relative to

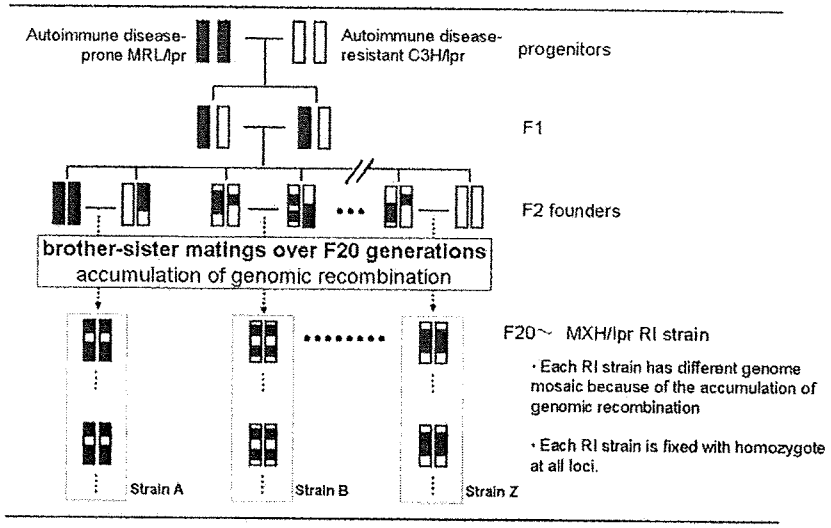

Fig. 1. How to establish recombinant inbred strains

marker	position (cM)	strains										
		6	7	10	21	25	28	36	41	43	51	54
D5Mit145	0	C	M	M	C	C	M	C	M	C	M	C
D5Mit74	11	C	C	M	C	C	C	C	M	C	M	C
D5Mit149	19	C	M	M	C	C	C	C	C	C	M	C
D5Mit233	29	M	C	C	C	C	C	M	C	C	C	C
D5Mit58	41	M	M	M	C	M	C	M	M	C	C	C
D5Mit115	56	M	M	M	M	M	C	M	C	C	C	C
D5Mit431	66	M	M	M	M	M	C	M	C	C	C	C
D5Mit33	78	C	C	M	M	C	C	M	C	M	C	C

Fig. 2. Strain distribution pattems of microsatellite loci in MXH/lpr RI strains. (samples of genome mosaic of the two progenitors) Each chromosome of RI strains had a different genome mosaic derived from the two progenitors, MRL/lpr and C3H/lpr. (M : MRL allele, C : C3H allele)

each other since the genome of each RI strain consists of a random combination of genomes.

The DNA derived from the original inbred parents as shown in Fig. 2. Identifying which part of a chromosome comes from genome DNA of the original inbred parents can be performed using DNA polymorphic markers. Thereafter, we will know which mutations are susceptible to the virulent phenotypes in RI strains of mice treated with chemicals, allowing for identification of some of the genomic mechanisms that play a role in selection.

ARSENIC TOXICITIES

In recent years, poisoning from arsenic caused by contamination of groundwater

and industrial exposure has been increasing. Arsenic toxicities are manifested as gastrointestinal symptoms (vomiting, diarrhea), arrhythmia, hyperkeratosis, cancer (skin, lung and urinary bladder), peripheral neuropathy, angiopathy and chronic hepatic and renal damage (Thomas *et al.*, 2001). These arsenic toxicities have been thought to appear based on a combination of exogenous factors such as the chemical forms of arsenic and the dose and the exposure period, and endogenous factors such as genetic backgrounds. This list suggests that such arsenic toxicities may thus be a polygenic trait.

In nature, arsenic exists in inorganic forms such as trivalent or pentavalent forms. The intake of inorganic arsenic is sequentially methylated as arsenic (MA), dimethylated arsenic (DMA) and trimetlylated arsenic (TMA) by glutathione S-transferase, and then excreted in urine. It is thought that trivalent forms have a greater toxicity than pentavalent forms, while inorganic forms have a higher toxicity than organic forms. Moreover, the capacity for arsenic methylation is known to vary among species. In humans, the variation of arsenic compounds such as inorganic arsenic, MMA and DMA have been observed (Vahter, 2000). Chiou *et al.* (1997) revealed that the polymorphism of glutathione S-transferase M1 and T1 influences the methylation capacity and the body retention of arsenic in Taiwanese populations. This report suggests that the variation in the capacity of arsenic metabolism and thereafter in the arsenic toxicities is regulated by genetic polymorphism.

Various arsenic toxicities have been observed and analyzed in relation to their molecular biology, using rodent experimental models. Evidence of several types of carcinogenesis from arsenic have been reported, for bladder cancer from organic arsenic compounds (Wanibuchi *et al.*, 2003), inorganic arsenic and lung cancer (Cui *et al.*, 2006), and inorganic arsenic combined with UV irradiation and skin cancer (Rossman *et al.*, 2004). The mechanism of carcinogenesis of arsenic compounds has recently been studied based on genotoxicity in association with oxidative DNA damage (Rossman, 2003). The effects of arsenic on the reproductive system and development (Holson *et al.*, 2000 ; Jana *et al.*, 2006), liver and brain damage (Mazumder, 2005 ; Bashir *et al.*, 2006), and cardiovascular disease (Simenova *et al.*, 2004 ; Saad *et al.*, 2006) has also been reported. Recently, the influence of arsenic compounds on the immune system has been highlighted because of the use of arsenic trioxide as a therapeutic agent for the treatment of acute promyelocytic leukemia (Chen *et al.*, 1997). Arsenic has been shown to increase lymphocyte apoptosis in the thymus and spleen, *in vitro* (Stepnik *et al.*, 2005), while also modulating the immune system (Bobe *et al.*, 2006). The genetic background of mouse strains also affects arsenic toxicities, as it similarly does in human beings.

For example, the acute toxicity (LD_{50}) of arsenic (Harrison *et al.*, 1958) and the susceptibility to arsenic-induced renal injury (Kimura *et al.*, 2005) differs among various mouse strains. As a result, a rodent experimental model is therefore considered necessary to analyze various arsenic toxicities based on genetics.

BENEFITS OF USING RI STRAINS IN THE GENETIC ANALYSIS OF ARSENIC TOXICITY

The major benefit of using mice in the analysis of arsenic toxicities is the ability to control genetic backgrounds in a simple experimental system. Many transgenic mice have been used in recent studies. However, genes are only candidates based on regular concepts, and only a few genes can be analyzed at a time. In order to study the polygenic traits induced by arsenic, it is necessary to take a 'statistic based' approach since polygenic traits are regulated by the combination of the multiple susceptibility of genes and environmental factors. Arsenic toxicities should also be evaluated as quantitative traits. As a result, the use of a QTL (quantitative trait loci) analysis is thus considered to be a suitable method for analyzing arsenic toxicities.

In general, to make a QTL analysis, hundreds of intercross (F2) or backcross (N2) mice derived from two progenitor strains are used. However, when evaluating environmental factors, genetic heterogeneity of the intercrossed mice makes it difficult to obtain reproducible results. Thus, a set of inbred strains having a genomic mosaic of progenitor strains, namely RI strains (Fig. 1 and 2), is considered a highly appropriate tool for analyzing the effect of environmental factors based on genomic polymorphism.

ARSENIC TOXICITY OF RI STRAINS

We analyzed acute arsenic toxicity in an RI strain called MXH/lpr, in which the progenitors were MRL/lpr and C3H/lpr strains. Each strain was administered doses of sodium metaarsenite per os at a half dose of LD_{50} (Kaise *et al.* 1985). Next, the mortality of these mice was observed at 8, 16, 24, 48 and 72 hrs after administration. As shown in Fig. 3, both progenitors revealed a high susceptibility to arsenic. The RI strains showed various levels of susceptibility to arsenic. This finding suggests that acute toxicity of arsenic is a polygenic trait, possibly having the genome combination derived from the progenitors, and involves its absorption from the alimentary tract, its effect on metabolism, and its toxicity on the terminal organs. In this way, we were thus able to find a highly resistant strain for acute arsenic toxicity, MXH28.

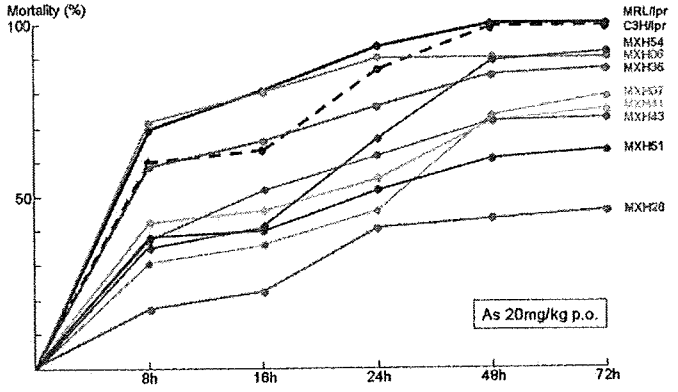

Fig. 3. Acute toxicity of arsenic in each strain of MXH/lpr

The intercross between arsenic-susceptible progenitors and an arsenic-resistant MXH/lpr strain showed a different susceptibility to acute arsenic toxicity. The (MXH28 x MRL/lpr) F1 mice revealed a high susceptibility (mortality 95%, 72 hrs after administration), while the (MXH28 x C3H/lpr) F1 mice tended to be resistant (mortality 63%, 72 hrs after administration). These results suggest that the major susceptible genes to acute arsenic toxicity are derived from an MRL/lpr allele. Based on a QTL analysis, the susceptibility loci were detected on chromosomes 13 and 15 at a suggestible level.

According to histopathological studies, the arsenic-administered mice showed erosion of the gastrointestinal tract and fatty changes in hepatocytes with a wide variation among strains (Fig. 4). Apoptosis of lymphocytes was observed in the MRL/lpr mice (Fig. 5), but such apoptosis was very weak in the C3H/lpr mice.

PROSPECTIVE

Our data clarified the fact that acute arsenic toxicity is regulated by a polygenic trait, as indicated by the genetic segregation of arsenic toxicity among the RI strains of MXH/lpr, in which both progenitors were highly susceptible to acute arsenic toxicity. Using a QTL analysis, we mapped the susceptibility loci on chromosomes 13 and 15. Moreover, RI strains were extended to study genetic variation by simply making an F1 generation derived from the cross between a progenitor and one of the RI strains, called a recombinant inbred intercross (RIX). RIX mice are thus expected to positively contribute to the investigations based on a QTL analysis. Therefore, the RI strains presented herein are expected to make it possible to detect novel genes susceptible to arsenic toxicity at a genome-wide level.

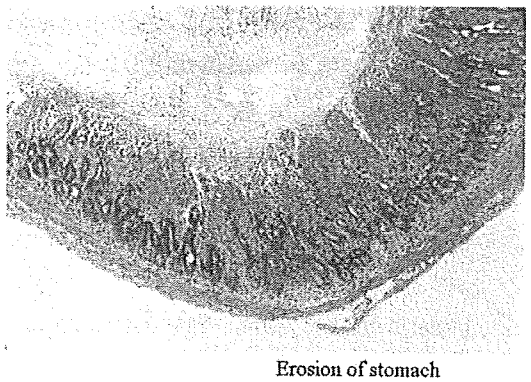

Erosion of stomach

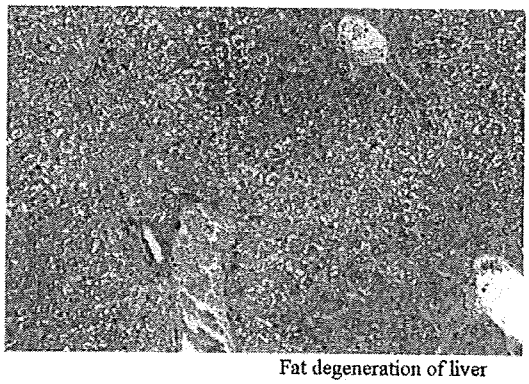

Fat degeneration of liver

Fig. 4. Representative histopahology of arsenic-administered mice (see Text) (As LD_{50} ½ 36 hrs)

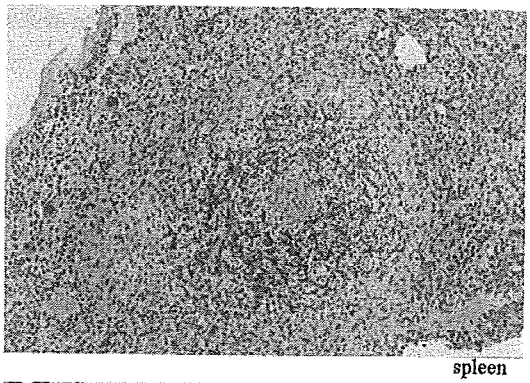

spleen

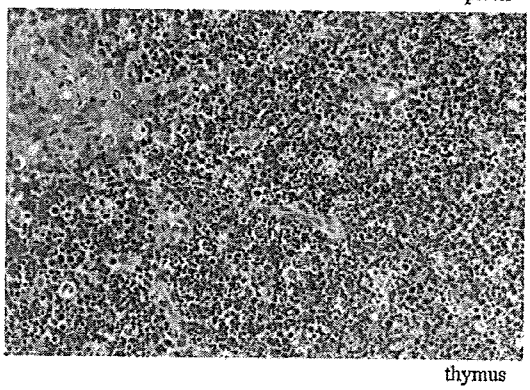

thymus

Fig. 5. The apoptosis of lymphocytes in the MRL/lpr mice

It is well known that some heavy metals disturb the immune system *in vivo* and also cause autoimmune diseases such as atopic diseases. MRL/lpr mice have the *lpr* gene, which is a deletion mutation of the F*as* gene. This mutation disrupts the negative selection of autoreactive lymphocytes, and causes the development of lymphoproliferation and autoimmune diseases in an MRL genetic background, associated with the accumulation of $B220^+Thy1.2^+$ double positive T cells, or so called lpr cells, to lymphatic tissue. Generally, mouse strains bearing the *lpr* gene (lpr mice) commonly show lymphoproliferation and autoimmune phenotypes. However, not all lpr mice develop autoimmune diseases because of their genetic background. As a result, the lpr gene can be designated an 'amplifier of autoimmune traits'. Bobe *et al.* (2006) revealed that administration of arsenic decreased lpr cells in MRL/lpr mice while ameliorating autoimmune disease phenotypes. In our studies, lymphocyte apoptosis was observed in MRL/lpr mice, but not significantly in either C3H/lpr or some MXH/lpr strains. These findings suggest that arsenic demonstrates immunotoxicity in the host immune system of lpr mice with different susceptibilities depending on genetic background. The RI strains with the *lpr* gene may also be useful for immnotoxicogenomics.

In this study using RI strains of mice, we showed that susceptibility to arsenic toxicities is inherited in a polygenic manner. Polygenes, which resulted from the accumulation of germ line mutations, seem to have a powerful potential for selection by toxic chemicals. The polymorphic structures and functions of these genes should therefore be studied further in the future.

REFERENCES

Bashir, S., Sharma, Y., Irshad, M., Gupta, S. D., Dogra, T. D., 2006. Arsenic-induced cell death in liver and brain of experimental rats. Basic Clinical Pharmacology and Toxicology 98 : 38-43.

Bobe, P., Bonardelle, D., Benihoud, K., Opolon, P., Chelbi-Alix, M. K., 2006. Arsenic trioxide, a novel promising therapeutic agent for lymphoproliferative and autoimmune syndromes in MRL/lpr mice. Blood 108 : 3967-3975.

Chen, G. Q., Shi, X. G., Tang, W., Xiong, S. M., Zhu, J., Cai, X., Han, Z. G., Ni, J. H., Shi, GY., Jia, P. M., Liu, M. M., He, K. L., Niu, C., Ma, J., Zhang, P., Zhang, T. D., Paul, P., Naoe, T., Kitamura, K., Miller, W., Waxman, S., Wang, Z. Y., de The, H., Chen, S. J., Chen, Z., 1997. Use of arsenic trioxide (As_2O_3) in the treatment of acute promyelocytic leukemia (APL) : I. As_2O_3 exerts dose-dependent dual effects on APL cells. Blood 89 : 3345-3353.

Chiou, H. Y., Hsueh, Y. M., Hsieh, L. L., Hsu, L. I., Hsu, Y. H., Hsieh, F. I., Wei, M. L., Chen, H. C., Yang, H. T., Leu, L. C., Chu, T. H., Chen-Wu, C., Yang, M. H., Chen, C. J., 1997. Arsenic methylation capacity, body retention, and null genotypes of glutathione S-transferase M1 and T1 among current arsenic-exposed residents in Taiwan. Mutation Research 386 : 197-207.

Cui, X., Wakai, T., Shirai, Y., Hatakeyama, K., Hirano,, S., 2006. Chronic oral exposure to inorganic arsenate interferes with methylation status of p16INK4a and RASSF1A and induces lung cancer in A/J mice. Toxicological Science 91 : 372-381.

Harrisson, J. W., Packman, E. W., Abbott, D. D., 1958. Acute oral toxicity and chemical and physical properties of arsenic trioxides. AMA Archives of Industrial Health 17 : 118-123.

Holson, J. F., Desesso, J. M., Jacobson, C. F., Farr, C. H., 2000. Appropriate use of animal models in the assessment of risk during prenatal development : an illustration using inorganic arsenic. Teratology 62 : 51-71.

Jana, K., Jana, S., Samanta, P. K., 2006. Effects of chronic exposure to sodium arsenite on hypothalamo-pituitary-testicular activities in adult rats : possible an estrogenic mode of action. Reproductive Biology and Endocrinology 4 : 9.

Kaise, T., Watanabe, S., Itoh, K,. 1985. The acute toxicity of arsenobetaine. Chemo-

sphere 14 : 1327-1332.
Kimura, A., Ishida, Y., Wada, T., Yokoyama, H., Mukaida, N., Kondo, T., 2005. MRP-1 expression levels determine strain-specific susceptibility to sodium arsenic-induced renal injury between C57BL/6 and BALB/c mice. Toxicology and Applied Pharmacology 203 : 53-61.
Mazumder, D. N., 2005. Effect of chronic intake of arsenic-contaminated water on liver. Toxicology and Applied Pharmacology 206 : 169-175.
Rossman, T. G., 2003. Mechanism of arsenic carcinogenesis : an integrated approach. Mutation Research 533 : 37-65.
Rossman, T. G., Uddin, A. N., Burns, F. J., 2004. Evidence that arsenite acts as a cocarcinogen in skin cancer. Toxicology and Applied Pharmacology 198 : 394-404.
Saad, S. Y., Alkharfy, K. M., Arafah, M. M., 2006. Cardiotoxic effects of arsenic trioxide/imatinib mesilate combination in rats. Journal of Pharmacy and Pharmacology 58 : 567-73.
Simeonova, PP., Luster, MI., 2004. Arsenic and atherosclerosis. Toxicology and Applied Pharmacology 198 : 444-449.
Stepnik, M., Stanczyk, M., Arkusz, J., Lewinska, D., 2005. Assessment of apoptosis in thymocytes and splenocytes from mice exposed to arsenate in drinking water : cytotoxic effects of arsenate on the cells in vitro. Journal of Environmental Science and Health Part A, Toxic Hazardous Substances and Environal Engineering 40 : 369-384.
Thomas, D. J., Styblo, M., Lin, S., 2001. The cellular metabolism and systemic toxicity of arsenic. Toxicology and Applied Pharmacology 176 : 127-144.
Vahter, M., 2000. Genetic polymorphism in the biotransformation of inorganic arsenic and its role in toxicity. Toxicological Letters 112-113 : 209-217.
Wanibuchi, H., Salim, E. I., Kinoshita, A., Shen, J., Wei, M., Morimura, K., Yoshida, K., Kuroda, K., Endo, G., Fukushima, S., 2004. Understanding arsenic carcinogenicity by the use of animal models. Toxicology and Applied Pharmacology 198 : 366-376.

Hiroaki Komori[1], *Yoshiko Soga*[1], *Shiro Mori*[2] *and Masato Nose*[1]
[1]*Department of Pathology, Ehime University Graduate School of Medicine, and*
[2]*Department of Oral Medicine and Surgery, Tohoku University Graduate School of Dentistry, Japan*
E-mail : *masanose@m.ehime-u.ac.jp*

Journal of Controlled Release 133 (2009) 198–205

Contents lists available at ScienceDirect

Journal of Controlled Release

journal homepage: www.elsevier.com/locate/jconrel

A novel strategy utilizing ultrasound for antigen delivery in dendritic cell-based cancer immunotherapy

Ryo Suzuki [a], Yusuke Oda [a], Naoki Utoguchi [a], Eisuke Namai [a], Yuichiro Taira [a], Naoki Okada [b], Norimitsu Kadowaki [c], Tetsuya Kodama [d], Katsuro Tachibana [e], Kazuo Maruyama [a,*]

[a] Department of Biopharmaceutics, School of Pharmaceutical Sciences, Teikyo University, 1091-1 Suwarashi, Sagamiko-cho, Sagamihara, Kanagawa 229-0195, Japan
[b] Department of Biotechnology and Therapeutics, Graduate School of Pharmaceutical Sciences, Osaka University, 1-6 Yamadaoka, Suita, Osaka 565-0871, Japan
[c] Department of Hematology and Oncology, Graduate School of Medicine, Kyoto University, 54 Shogoin Kawara-cho, Sakyo-ku, Kyoto 606-8507, Japan
[d] Department of Biomedical Engineering, Graduate School of Biomedical Engineering, Tohoku University, 2-1 Seiryo-machi, Aoba-ku, Sendai 980-8575, Japan
[e] Department of anatomy, School of medicine, Fukuoka University, 7-45-1 Nanakuma, Jonan-ku, Fukuoka 814-0180, Japan

ARTICLE INFO

Article history:
Received 12 August 2008
Accepted 16 October 2008
Available online 31 October 2008

Keywords:
Dendritic cells
Antigen delivery system
Cancer immunotherapy
Ultrasound
Liposomes

ABSTRACT

In dendritic cell (DC)-based cancer immunotherapy, it is important that DCs present peptides derived from tumor-associated antigens on MHC class I, and activate tumor-specific cytotoxic T lymphocytes (CTLs). However, MHC class I generally present endogenous antigens expressed in the cytosol. We therefore developed an innovative approach capable of directly delivering exogenous antigens into the cytosol of DCs; i.e., a MHC class I-presenting pathway. In this study, we investigated the effect of antigen delivery using perfluoropropane gas-entrapping liposomes (Bubble liposomes, BLs) and ultrasound (US) exposure on MHC class I presentation levels in DCs, as well as the feasibility of using this antigen delivery system in DC-based cancer immunotherapy. DCs were treated with ovalbumin (OVA) as a model antigen, BLs and US exposure. OVA was directly delivered into the cytosol but not via the endocytosis pathway, and OVA-derived peptides were presented on MHC class I. This result indicates that exogenous antigens can be recognized as endogenous antigens when delivered into the cytosol. Immunization with DCs treated with OVA, BLs and US exposure efficiently induced OVA-specific CTLs and resulted in the complete rejection of E.G7-OVA tumors. These data indicate that the combination of BLs and US exposure is a promising antigen delivery system in DC-based cancer immunotherapy.

1. Introduction

Dendritic cells (DCs), which are unique antigen-presenting cells capable of priming naive T cells, are promising vaccine carriers for cancer immunotherapy [1]. To induce efficiently a tumor-specific cytotoxic T-lymphocyte (CTL) response, DCs should abundantly present epitope peptides derived from tumor-associated antigens (TAAs) via major histocompatibility complex (MHC) class I molecules [2]. In general, the majority of peptides presented via the MHC class I molecules are generated from endogenously synthesized proteins that are degraded by the proteasome [3]. On the other hand, exogenous antigens such as TAAs for DCs are preferentially presented on MHC class II molecules [3]. In order to prime efficiently TAAs specific for CTLs, it is important to develop a novel antigen delivery system, which can induce MHC class I restricted TAA presentation on DCs. Several researchers are developing antigen delivery tools based on the cross presentation theory of exogenous antigens for DCs [4–8]. In these studies, various types of antigen delivery carriers such as liposomes [6,7], poly(γ-glutamic acid) nanoparticles [5] and cholesterol pullulan nanoparticles [8], all of which can deliver antigen into DCs via the endocytosis pathway, have been developed. We have reported that IgG modified liposomes with entrapped antigen can induce cross presentation of exogenous antigen for DCs on MHC class I molecules [9]. These carriers deliver antigens into DCs via an endocytosis mechanism, with delivery thought to be due to exogenous antigen leaking from the endosome into the cytosol. It is therefore important to design an antigen delivery system which does not rely on the endocytosis pathway. In other study, it was reported that DCs pulsed with exogenous antigens by electroporation presented their antigens on MHC class I molecules and resulted

Abbreviations: Alexa-OVA, Alexa Fluor 488-conjugated ovalbumin; BL, Bubble liposome; CTL, cytotoxic T lymphocyte; DC, dendritic cell; DSPC, 1,2-distearoyl-sn-glycero-phosphatidylcholine; DSPE-PEG(2k)-OMe, 1,2-distearoyl-sn-glycero-3-phosphatidyl-ethanolamine-methoxypolyethyleneglycol; ER, endoplasmic reticulum; FBS, fetal bovine albumin; HLA, human leukocyte antigen; MHC, major histocompatibility complex; MTT, 3-(4,5-s-dimethylthiazol-2-yl)-2,5-diphenyl tetrazolium bromide; NaN_3, sodium azide; OVA, ovalbumin; PBS, phosphate buffer saline; US, ultrasound; TAA, tumor associated antigen.

* Corresponding author. Department of Biopharmaceutics, School of Pharmaceutical Sciences, Teikyo University, 1091-1 Suwarashi, Sagamiko-cho, Sagamihara, Kanagawa 229-0195, Japan. Tel.: +81 42 685 3722; fax: +81 42 685 3432.
E-mail address: maruyama@pharm.teikyo-u.ac.jp (K. Maruyama).

0168-3659/$ – see front matter © 2008 Elsevier B.V. All rights reserved.
doi:10.1016/j.jconrel.2008.10.015

in inducing MHC class I-mediated antitumor immunity. Although electroporation is commonly utilized as gene delivery method and deliver gene such as DNA and RNA into cytosol, Kim K.W. et al and Weiss J.M. et al. apply this system to antigen delivery into DCs [10,11]. Their reports also demonstrate the importance of delivering exogenous antigens into cytosol of DCs to induce MHC class I presentation of the antigens.

It has been reported that ultrasound (US) increases the permeability of the plasma membrane, which encourages the entry of DNA into cells [12,13]. The first studies applying US for gene delivery used frequencies in the range of 20–50 kHz [12,14]. However, these frequencies, along with cavitation, are also known to induce tissue damage if not properly controlled [15–17]. To address this problem, many studies into using therapeutic US for gene delivery have used frequencies of 1–3 MHz, intensities of 0.5–2.5 W/cm^2 and a pulse-mode [18–20]. In addition, it was reported that the combination of therapeutic US and microbubble echo contrast agents could enhance gene transfection efficiency [21–27]. In this method, DNA is effectively and directly transferred into the cytosol. This system has been applied to deliver proteins into cells [28,29], but not yet to deliver antigens into DCs for the purpose of cancer immunotherapy. Previously, we developed novel liposomal bubbles containing nanobubbles of the US imaging gas, perfluoropropane [30–34] and suggested that these "Bubble liposomes" (BLs) might be used as novel non-viral gene delivery tools if combined with US exposure. In the case of DCs, the antigen delivered into the cytosol would present on MHC class I molecules and result in priming antigen-specific CTLs. In this study, we examined the effectiveness of BLs combined with US exposure to deliver antigen into DCs. In addition, the effectiveness of this antigen delivery system in DC-based cancer immunotherapy was assessed.

2. Materials and methods

2.1. Cells

T cell hybridoma CD8-OVA1.3 (a kind gift from Dr. C.V. Harding, Department of Pathology, Case Western Reserve University, Cleveland, OH, USA), a cell type that recognizes SIINFEKL:H-2K^b complexes [35], was cultured in Dulbecco's modified Eagle's medium (DMEM, Sigma Chemical Co., St. Louis, MO, USA) supplemented with 10% heat inactivated fetal bovine serum (FBS, GIBCO, Invitrogen Co., Carlsbad, CA, USA), 50 μM 2-mercaptethanol (2-ME), 250 μg/ml amphotericin B (Wako Pure Chemical Industries, Ltd., Osaka, Japan) and 50 μg/ml gentamycin (Wako Pure Chemical Industries). EL-4 murine thymoma cells were cultured in RPMI 1640 supplemented with 10% FBS and 50 μM 2-ME. E.G7-OVA cells (OVA cDNA transfectant of EL4 cells) were maintained in RPMI 1640 supplemented with 10% FBS, 50 μM 2-ME and 400 μg/ml GENETICIN (G418 sulfate, GIBCO, Invitrogen). All culture media contained 50 U/ml penicillin and 50 μg/ml streptomycin (Wako Pure Chemical Industries).

2.2. Generation of mouse bone marrow-derived DCs

DCs were generated from bone marrow cells as described elsewhere [36]. Briefly, bone marrow cells were isolated from C57BL/6 mice and were cultured in RPMI 1640 with 10% FBS, 50 U/ml penicillin, 50 μg/ml streptomycin and 40 ng/ml mouse granulocyte-macrophage colony-stimulating factor (GM-CSF). After 8–16 days of culture, non-adherent cells were collected and used as DCs.

2.3. Preparation of BLs

Liposomes composed of 1,2-distearoyl-sn-glycero-phosphatidylcholine (DSPC) (NOF Corp., Tokyo, Japan) and 1,2-distearoyl-sn-glycero-3-phosphatidyl-ethanolamine-methoxypolyethyleneglycol (DSPE-PEG(2k)-OMe, (PEG Mw=ca. 2000), NOF) (94 : 6 (m/m)) were prepared by reverse phase evaporation. Briefly, all reagents (total lipid: 100 μmol) were dissolved in 8 ml of 1:1 (v/v) chloroform/diisopropyl ether, then 4 ml of phosphate buffered saline (PBS) was added. The mixture was sonicated and evaporated at 65 °C. The solvent was completely removed, and the size of the liposomes was adjusted to less than 200 nm using an extruding apparatus (Northern Lipids Inc., Vancouver, BC, Canada) and sizing filters (pore sizes: 100 and 200 nm; Nuclepore Track-Etch Membrane, Whatman plc, UK). After sizing, the liposomes were sterilized by passing them through a 0.45 μm pore size filter (MILLEX HV filter unit, Durapore PVDF membrane, Millipore Corp., MA, USA). The size of the liposomes was measured by dynamic light scattering (ELS-800, Otsuka Electronics Co., Ltd., Osaka, Japan). The average diameter of these liposomes was between 150–200 nm. Lipid concentration was measured using the Phospholipid C test (Wako Pure Chemical Industries). BLs were prepared from the liposomes and perfluoropropane gas (Takachiho Chemical Industrial Co., Ltd., Tokyo, Japan) [31,33]. Briefly, 5 ml sterilized vials containing 2 ml of the liposome suspension (lipid concentration: 2 mg/ml) were filled with perfluoropropane, capped, and then supercharged with 7.5 ml of perfluoropropane. The vial was placed in a bath-type sonicator (42 kHz, 100 W; BRANSONIC 2510J-DTH, Branson Ultrasonics Co., Danbury, CT, USA) for 5 min to form the BLs. In this method, the liposomes were reconstituted by sonication under the condition of supercharge with perfluoropropane in the 5 mL vial container. At the same time, perfluoropropane would be entrapped within lipids like micelles, which were made by DSPC and DSPE-PEG(2k)-OMe from liposome composition, to form nanobubbles. The lipid nanobubbles were encapsulated within the reconstituted liposomes, which sizes were changed into around 1 μm from 150–200 nm of original.

2.4. Antigen trafficking into DCs after antigen delivery with BLs and US exposure

Alexa Fluor 488 conjugated OVA (Alexa-OVA) was prepared with Alexa Fluor 488 succinimidyl ester (Molecular Probes, Invitrogen) according to the instruction manual. DCs (1×10^5 cells/ml) were cultured in a glass bottom dish (IWAKI, Asahi Glass Co. Ltd., Tokyo, Japan) overnight. After washing the cells with OptiMEM (Invitrogen), BLs (240 μg/ml) and Alexa-OVA (50 μg/ml) were added to the dish. Then, the DCs were exposed to US exposure (frequency: 2 MHz, duty: 10%, burst rate: 2.0 Hz, intensity 2.0 W/cm^2, time: 3×10 s (interval: 10 s)) using a Sonopore 4000 (6 mm diameter probe; Nepa Gene Co. Ltd., Chiba, Japan). This condition was decided referring to our reports about gene delivery [31,33] and Guo et al.'s report about the repeat US exposure with interval [37], and from the viewpoint of cytotoxicity for DCs. After US exposure, the DCs were incubated for 1 h at 37 °C, then washed with PBS, fixed with 3% paraformaldehyde for 10 min, and treated with 0.1% Triton X-100 (Wako Pure Chemical Industries) for 5 min. In addition, some DCs were washed with PBS, their nuclei were stained with propidium iodide (0.5 μg/ml) (Wako Pure Chemical Industries), and antigen trafficking was observed with a confocal laser microscope.

2.5. Antigen delivery following inhibition of the endocytosis pathway in DCs

DCs were pretreated with OptiMEM containing 10 mM NaN_3 for 1 h at 4 °C to inhibit the endocytosis pathway. After washing the cells, BLs (240 μg/ml) and Alexa-OVA (50 μg/ml) were added to the DCs in OptiMEM containing 10 mM sodium azide (NaN_3). The DCs were exposed to US exposure (frequency: 2 MHz, duty: 10%, burst rate: 2.0 Hz, intensity 2.0 W/cm^2, time: 3×10 s (interval: 10 s)), then washed with PBS containing10 mM NaN_3. After US exposure, DCs were fixed and their nuclei were stained as described above (2.4.).

2.6. Flow cytometry analysis of antigen delivery into DCs with BLs and US exposure

Alexa-OVA was delivered into DCs under inhibited endocytosis conditions as described above (2.5.). After washing, the DCs were stained with propidium iodide (100 ng/ml) and analyzed by flow cytometry (FACSCalibur, Becton, Dickinson and Company, Franklin Lakes, NJ, USA). In this study, living DCs (1×10^4 cells) were analyzed by gating out propidium iodide staining cells.

2.7. Assessment of MHC class I restricted OVA presentation

DCs (2.5×10^5 cells/500 μl/well (48-well plate)) were pulsed with OVA alone (0, 10, 100, 1000 μg/ml) or OVA (0, 10, 100, 1000 μg/ml) using US exposure (frequency: 2 MHz, duty: 10%, burst rate: 2.0 Hz, intensity 2.0 W/cm^2, Time: 3×10 s (interval: 10 s)) and/or BLs (240 μg/ml). After US exposure, the DCs were incubated for 1 h at 37 °C, then washed with PBS. After culturing for 24 h, the DCs were co-cultured for 20 h with T cell hybridoma CD8-OVA1.3 (2×10^5 cells/well) that recognizes SIINFEKL: H-2K^b complexes. The concentration of IL-2 in the supernatants was measured using an IL-2 ELISA Kit (BioSource International, Inc., Camarillo, CA, USA).

2.8. Assessment of cytotoxicity to DCs by the treatment of BLs and US exposure

DCs (2.5×10^5 cells/500 μl/well (48-well plate)) were treated with BLs (240 μg/ml) and/or US exposure (frequency: 2 MHz, duty: 10%, burst rate: 2.0 Hz, intensity 2.0 W/cm^2, Time: 3×10 s (interval: 10 s)). After US exposure, DCs were incubated for 1 h at 37 °C, and washed with PBS. The DCs were resuspended with cuture medium (250 μl) and cultured for 48 h. Cell viability was assayed using MTT (3-(4,5-s-dimethylthiazol-2-yl)-2,5-diphenyl tetrazolium bromide, Dojindo, Kumamoto, Japan) as described by Mosmann with minor modifications [38]. Briefly, MTT (5 mg/mL, 25 μL) was added to each well and the cells were incubated at 37 °C for 4 h. The formazan product was dissolved in 250 μL of 10% sodium dodecyl sulfate (SDS, Wako Pure Chemical Ind. Co., Ltd. Osaka, Japan) containing 15 mM HCl. Color intensity was measured using a microplate reader (POWERSCAN HT; Dainippon Pharmaceutical, Osaka, Japan) at test and reference wavelengths of 595 and 655 nm, respectively.

2.9. Immunization of mice with DCs and cytotoxicity assay

DCs (2.5×10^5 cells/500 μl/well) were pulsed with OVA alone (100 μg/ml) or OVA (100 μg/ml) using US exposure (frequency: 2 MHz, duty: 10%, burst rate: 2.0 Hz, intensity 2.0 W/cm^2, Time: 3×10 s (interval: 10 s)) and/or BLs (240 μg/ml) on a 48-well plate, then collected from 10 wells and seeded into 6-well plates. After 1 h incubation at 37 °C, the DCs were washed and cultured for 24 h at 37 °C. After washing, DCs (1×10^6 cells/100 μl) were intradermally injected into the backs of C57BL/6 mice. After 7 days, the mice were re-immunized. Seven days after the second immunization, splenocytes were obtained from five mice, and the splenocytes were pooled and stimulated with mitomycin C-treated E.G7-OVA cells at a ratio of 10:1 for 5 days. The stimulated splenocytes were used as effector cells for the cytotoxicity assay, using EL-4 or E.G7-OVA as the target cells in a flow cytometric assay employing two fluorochromes [39]. PKH-67, a fluorochrome which fluoresces green, binds to the cytoplasmic membrane and does not leak or transfer, was used to identify the target cell population. Propidium iodide fluoresces red and was used to detect non-viable cells. Use of these two fluorochromes and two parameter analyses allowed the identification of four subpopulations in the sample: live effectors, dead effectors, live targets and dead targets. By enumerating these subpopulations, the percent target lysis can be calculated.

2.10. Antitumor effect by prior immunization with antigen-pulsed DCs

DCs (2.5×10^5 cells/500 μl/well) were pulsed with OVA alone (100 μg/ml) or OVA (100 μg/ml) using US exposure (frequency: 2 MHz, duty: 10%, burst rate: 2.0 Hz, intensity 2.0 W/cm^2, Time: 3×10 s (interval: 10 s)) and/or BLs (240 μg/ml) on a 48-well plate, then collected from 10 wells and seeded into 6-well plates. After 1 h incubation at 37 °C, the DCs were washed and cultured for 24 h at 37 °C. After washing, the DCs (1×10^6 cells/100 μl) were intradermally immunized into the backs of C57BL/6 mice twice at intervals of one week. Seven days after the second immunization, E.G7-OVA cells (1×10^6 cells) were intradermally inoculated into the backs of mice and the size of the tumors was monitored using the formula: (major axis×minor axis^2)×0.5. All treated groups contained five mice.

2.11. Re-challenge of tumor cells

E.G7-OVA cells (1×10^6 cells) were injected into mice that were resistant to tumor cells due to immunization with DCs treated with BLs, US exposure and OVA. Untreated mice were used as controls to confirm the development of cancer following the first inoculation with E.G7-OVA cells. All treated groups contained five mice.

2.12. Treatment of tumor-bearing mice with antigen-pulsed DCs

E.G7-OVA cells (1×10^6 cells) were intradermally inoculated into the backs of C57BL/6 mice. On day 9, when the tumors were between 8–10 mm, OVA pulsed DCs (1×10^6 cells) prepared as described above were intradermally injected into the backs of the mice. On day 12, DCs were injected similarly. Tumor sizes were monitored from the day of inoculation. All treated groups contained five mice.

2.13. Statistical analysis

Differences in IL-2 secretion between the experimental groups were compared using non-repeated measures ANOVA and Dunnett's test.

3. Results

3.1. Antigen delivery by BLs and sonoporation into the cytosol of DCs lacking the endocytosis pathway

We examined antigen trafficking following delivery using a combination of BLs and US exposure (Fig. 1(a)). In DCs treated with Alexa-OVA in the presence or absence of either BLs or US exposure, the fluorescence from Alexa-OVA appeared as dots in the cytosol. On the other hand, in DCs treated with Alexa-OVA, BLs and US exposure, the fluorescence appeared as dots, but also as diffused fluorescence in the cytosol. To confirm this, antigen delivery was examined following inhibition of the endocytosis pathway in DCs by treatment with sodium azide (Fig. 1(b)). In DCs treated with Alexa-OVA either with or without BLs or US exposure, the fluorescence derived from Alexa-OVA was not observed. On the other hand, in DCs treated with Alexa-OVA, BLs and US exposure, fluorescence was observed in the cytosol even when the endocytosis pathway in DCs was inhibited. In addition, the efficiency of antigen delivery following inhibition of the endocytosis pathway was assessed using flow cytometory (Fig. 1(c)). The fluorescence intensity of DCs treated with Alexa-OVA, BLs and US exposure was higher than that of DCs treated with Alexa-OVA alone, or of Alexa-OVA and BLs or US exposure. These data support the data shown in Fig. 1(b), indicating that Alexa-OVA is observed in the cytosol when DCs are only treated with BLs and US exposure, even when the endocytosis pathway is

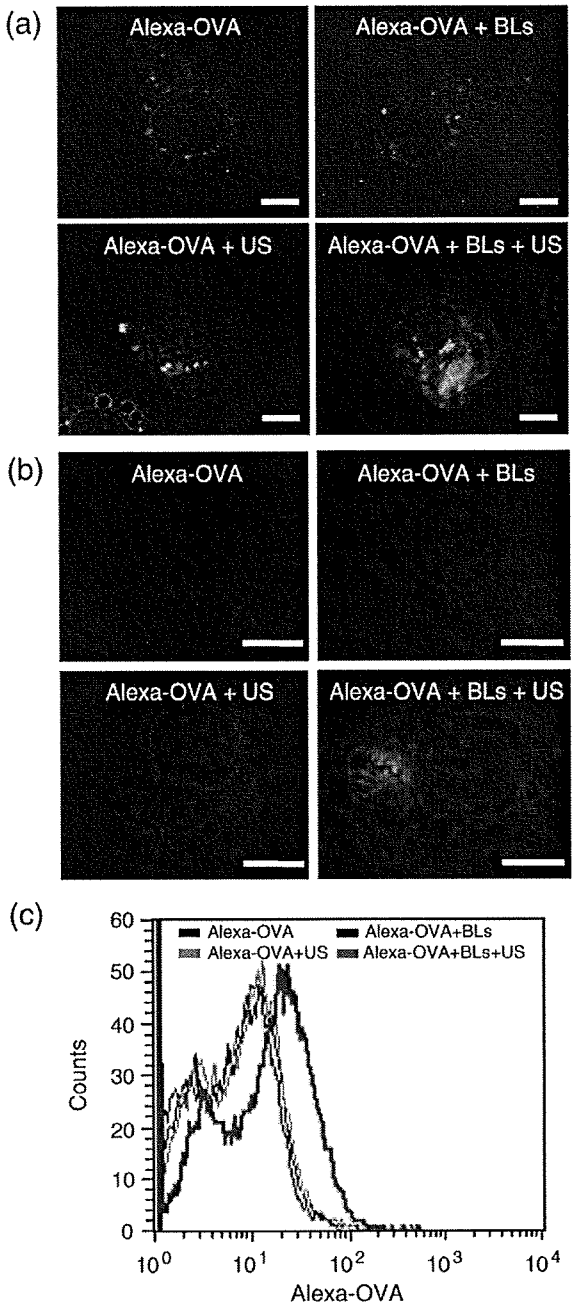

Fig. 1. Intracellular antigen delivery into DCs using BLs and US exposure. (a) Uptake of Alexa-OVA into DCs. DCs were cultured in a glass bottom dish overnight. After washing the cells, Alexa-OVA was added to the dish. Then, the DCs were exposed to US in the presence or absence of BLs and incubated for 1 h at 37 °C. The DCs were washed with PBS, fixed, and the nuclei were stained with propidium iodide. The uptake of Alexa-OVA was observed using a confocal laser microscope. (b) Intracellular delivery of Alexa-OVA into DCs using BLs and US. DCs were pretreated with OptiMEM containing 10 mM NaN_3 for 1 h at 4 °C to inhibit the endocytosis pathway. After washing the cells, Alexa-OVA was added to the DCs in OptiMEM containing10 mM NaN_3. Then, the DCs were exposed to US in the presence or absence of BLs. After US exposure, the DCs were washed with PBS containing 10 mM NaN_3, fixed, and the nuclei were stained with propidium iodide. Intracellular trafficking of Alexa-OVA in the DCs was observed using a confocal laser microscope. Scale bar shows 5 μm. (c) Flow cytometry analysis of DCs containing Alexa-OVA delivered using BLs and US. Alexa-OVA was delivered into the cell interior of the DCs during endocytosis inhibition. After washing the cells, the DCs were analyzed by flow cytometry.

inhibited. These results suggest that the combination of BLs and US exposure can be used to directly deliver antigens into the cytosol of DCs in the absence of endocytosis.

3.2. MHC class I presentation of exogenous antigen delivered into DCs by BLs and US exposure

Exogenous antigen delivered into the cytosol of DCs by BLs and US exposure is recognized as endogenous antigen by DCs and leads to the efficient presentation of peptides derived from exogenous antigens on MHC class I molecules. Thus, we examined whether antigen delivery by BLs and US exposure resulted in the efficient presentation of peptides on MHC class I molecules and the stimulation of $CD8^+$ T cells. C57BL/6-derived OVA-specific T cell hybridoma CD8-OVA1.3 was co-cultured with mouse bone marrow-derived DCs pulsed with antigen. As shown in Fig. 2, CD8-OVA1.3 cells stimulated with DCs pulsed with soluble OVA, either treated or untreated by BLs or US exposure did not secrete a significant amount of IL-2. Of note, a larger amount of IL-2 was secreted by CD8-OVA1.3 cells stimulated with DCs pulsed with OVA treated with a combination of BLs and US exposure. These data indicate that antigen delivery by BLs to DCs upon sonoporation results in the presentation of peptides derived from OVA on MHC class I molecules. In this data, the level of IL-2 secretion increased depending on OVA concentration and reached plateau in 100 μg/ml of OVA concentration. Therefore, we used this OVA concentration (100 μg/ml) in further examinations.

3.3. Cytotoxicity to DCs by the treatment of BLs and US exposure

In this antigen delivery system using BLs and US exposure, the transient pores would be provided on the membrane of DCs. Therefore, it is concerned that the DCs are injured by US exposure in the presence of BLs. To assess the cytotoxicity to DCs by the treatment of BLs and US exposure, we examined about the viability of DCs (Fig. 3). In the treatment of DC with BLs and/or US exposure, the viability of DCs treated with BLs, US exposure or BLs/US exposure was 83 ± 11%, 96 ± 5% or 87 ± 13%, respectively. This result shows that there is not serious damage to DCs even under the condition of inducing transient pores on the membrane of DCs treated with BLs and US exposure.

3.4. Induction of antigen-specific CTL response in the immunization of DCs pulsed with antigen using BLs and US exposure

To examine whether efficient peptide presentation on MHC class I molecules leads to strong induction of antigen-specific CTLs *in vivo*, we immunized C57BL/6 mice twice with bone marrow-derived DCs that had been treated with various antigen delivery techniques. Thereafter, splenocytes were isolated, and a cytotoxicity assay was

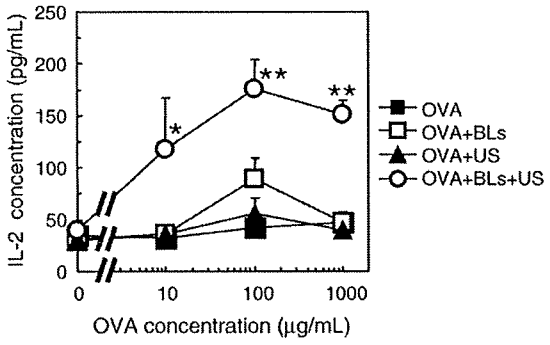

Fig. 2. MHC class I restricted OVA presentation after OVA delivery into DCs using a combination of BLs and US exposure. DCs were pulsed with OVA alone or OVA in conjunction with US exposure and/or BLs. After US exposure, the DCs were incubated for 1 h at 37 °C, then washed with PBS. After culturing for 24 h, the DCs were co-cultured with CD8-OVA1.3 cells for 20 h. The concentration of IL-2 in the supernatants was measured. Each data represents the mean ± S.D. for triplicate measurements. *$P<0.05$ compared to the group treated with BLs or US, or without BLs and US. **$P<0.01$ compared to the group treated with BLs or US, or without BLs and US.

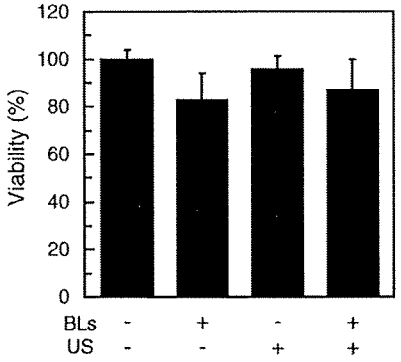

Fig. 3. Viability of DCs treated with BLs and /or US exposure. DCs were treated with BLs and/or US. After US exposure, DCs were incubated for 1 h at 37 °C, then washed with PBS. After culturing for 48 h, the viability of DCs was measured by MTT assay. Each data represents the mean±S.D. for triplicate measurements.

performed using the syngeneic lymphoma cell line EL-4 or its OVA transfectant, E.G7-OVA. As shown in Fig. 4, immunization with DCs without OVA, DCs pulsed with OVA, or OVA combined with BLs or US exposure, induced weak cytotoxicity of splenocytes against the OVA-expressing cell line E.G7-OVA. In contrast, immunization with DCs pulsed with OVA following BL and US exposure resulted in strong cytotoxicity against the OVA-expressing cell line E.G7-OVA by splenocytes. Splenocytes from mice immunized with DCs pulsed using any method of antigen delivery did not exhibit strong cytotoxicity against the parental cell line EL-4. These data indicate that DCs pulsed with antigen using BLs and US exposure as the antigen delivery method efficiently present peptides on MHC class I molecules, which results in strong induction of antigen-specific CTLs *in vivo*.

3.5. Antitumor effects in the immunization of DCs pulsed with antigen by BLs and US exposure

Using an E.G7-OVA tumor model, we examined whether the strong induction of CTLs by antigen delivery with BLs and US exposure leads to efficient anti-tumor immune responses *in vivo*. We immunized C57BL/6 mice twice with bone marrow-derived DCs that had been pulsed using one of two methods of antigen delivery (OVA with US exposure, or OVA with BLs and US exposure). One week after the second immunization, the mice were inoculated intradermally with E.G7-OVA cells, and tumor growth was monitored. As shown in Fig. 5(a) and (b), immunization with untreated DCs weakly suppressed tumor growth. The survival rate of mice immunized with untreated DCs was slightly prolonged, suggesting that non-specific inflammatory responses induced by the injection of DCs result in weak anti-tumor immune responses. Immunization with DCs that had been pulsed with OVA using US exposure suppressed tumor growth slightly more efficiently than the control immunization. Of note, immunization with DCs that had been pulsed with OVA using BLs and US exposure completely suppressed tumor growth, with all mice in this group surviving more than 70 days after tumor inoculation. In addition, we examined the prevention of tumor growth recurrence after re-inoculation of tumor cells into mice, which had completely rejected the first injection of tumor cells (Fig. 5(c)). All mice, which were re-inoculated with E.G7-OVA cells 10 weeks after the first inoculation, completely rejected the tumor cells.

Finally, we examined whether immunization with DCs pulsed with antigen using BLs and US exposure can efficiently suppress the growth of established tumors. For this purpose, we inoculated C57BL/6 mice with E.G7-OVA, and after 9 and 12 days, when the tumors were between 100–200 mm^3, DCs were injected intradermally. As shown in Fig. 6(a), administration of untreated DCs did not provide a significant therapeutic effect. Administration of DCs pulsed with OVA using US exposure exhibited a weak therapeutic effect. Importantly, administration of DCs pulsed with OVA using BLs and US exposure exhibited stronger therapeutic effects in two of the five mice, with these two mice surviving for more than 60 days (Fig. 6(b)). These data indicate that antigen delivery into DCs with BLs and US exposure can induce significant therapeutic effects on established tumors.

4. Discussion

Subunit vaccines utilizing MHC class I-binding peptides have significant limitations that hinder their application to the general patient population (restrictions of HLA types) and that also affect their clinical effectiveness (monovalency of tumor specific antigen) in DC-based tumor immunotherapy. Utilization of tumor associated proteins as antigens may overcome this limitation, thereby enabling a broad spectrum of peptide presentation. In fact, patients treated with tumor cell lysates pulsed DCs showed better response rates compared with patients treated with peptide pulsed DCs [40]. This clinical trial suggests that tumor lysates are a good source of tumor antigens for a polyvalent antitumor vaccine. On the other hand, MHC class I molecules generally present endogenous antigens, whereas exogenous antigens for DCs are taken up by the endocytosis pathway and exogenous antigen-derived peptides are presented on MHC class II molecules [3]. In this study, we showed that by using a combination of BLs and US exposure, exogenous antigen was directly delivered into the cytosol of DCs (Fig. 1) and was presented on MHC class I molecules (Fig. 2). In addition, DCs immunized with antigen delivered by BLs and US exposure could stimulate antigen-specific CTL activation (Fig. 4) and resulted in inducing effective anti-tumor immune responses in tumor-bearing mice. (Figs. 5 and 6) Although peptide and protein delivery with sonoporation using microbubbles have been previously reported [28,29,41], the present study is the first report of effective antigen delivery into DCs by BLs using sonoporation for cancer immunotherapy.

Sonoporation and microbubbles such as Optison have been reported to be an effective gene delivery method using non-viral vectors. In addition, peptide and protein delivery with microbubbles and US exposure has been reported [28,29,41]. In the reports, Bekeredjian et al. showed the feasibility of microbubbles and US exposure for delivery of bioactive protein (luciferase, 60 kDa) into the cytosol of *in vitro* and *in vivo* cells [28,29]. Larina I.V. et al. reported that FITC-dextrans of 10–2000 kDa were delivered into human breast

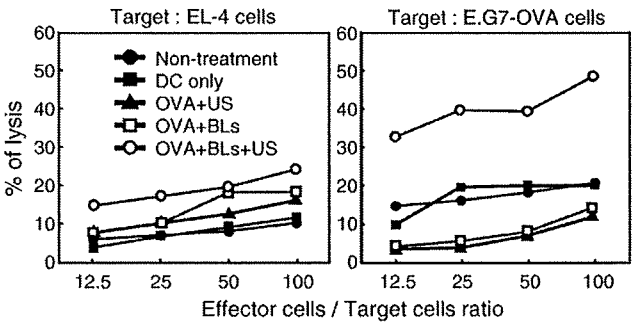

Fig. 4. Antigen specific CTL induction after immunization with DCs treated with BLs and US exposure. DCs were pulsed with OVA under each condition and cultured. After washing the cells, the DCs were intradermally injected into the backs of C57BL/6 mice. After 7 days, the mice were re-immunized. Seven days after the second immunization, splenocytes were obtained and stimulated with mitomycin C-treated E.G7-OVA cells at a ratio of 10:1 for 5 days. The stimulated splenocytes were used as effector cells for a cytotoxicity assay, using EL-4 or E.G7-OVA cells as the target in a flow cytometric assay.

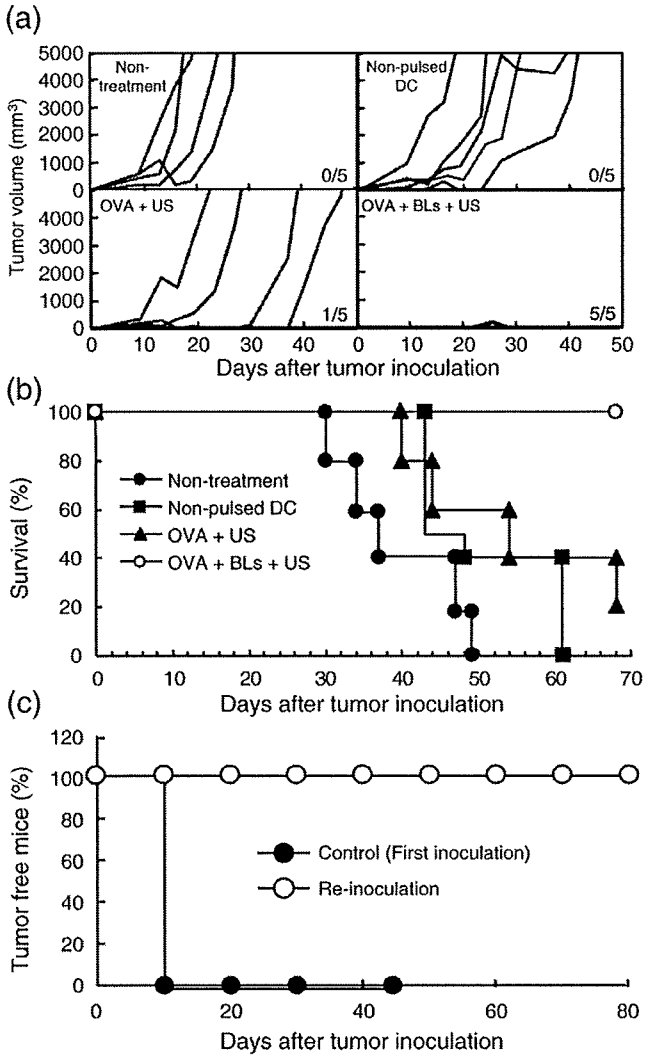

Fig. 5. Antitumor effect caused by immunization of DCs treated with antigen, BLs and US exposure. C57BL/6 mice were immunized with DCs twice. Seven days after the second immunization, E.G7-OVA cells were intradermally inoculated into the backs of the mice, and the tumor volume and survival of the mice was monitored. (a): Tumor volume of the mice after tumor inoculation. Each line indicates the tumor volume in an individual mouse. The fractional number in the lower right of each group shows the number of mice completely rejecting tumors / the number of total experimental mice. (b): Survival rate of the mice after tumor inoculation. (c): Tumor rejection efficiency after re-inoculation with tumor cells. E.G7-OVA cells were re-injected into the mice, which had rejected tumor cells following immunization with DCs treated with OVA, BLs and US in a prior immunization (a). Normal mice were used as controls to confirm the development of cancer following the first inoculation with E.G7-OVA cells. All treated groups contained five mice.

adenocarcinoma (MCF7) by the combination of Optison (conventional microbubbles) and US exposure [42]. It is believed that the delivery mechanism is due to the presence of transient pores through the cell membrane, resulting in extracellular molecules being directly delivered into the cytosol [22,43]. As shown in Fig. 1(b), antigen was directly delivered into DCs by the combination of BLs and US exposure even when the endocytosis pathway was inhibited. Therefore, it is thought that the antigen delivery mechanism induced by BLs and sonoporation is the same as that induced by microbubbles and sonoporation. In studies using microbubbles and sonoporation, pore sizes (based on the physical diameter of the component compounds) were typically between 30–100 nm, and estimates of the membrane recovery time ranged from a few seconds to a few minutes [44]. On the other hand, in studies on the aftereffects of US exposure on cell membranes, Eshet *et al.* reported that microbubbles resulted in a rougher cell surface characterized by depressions, but that the effects are reversible within 24 h following US exposure [43]. In the present study, DCs were incubated with antigen for 1 h after US exposure and increased the delivery efficiency of antigen into the cytosol of DCs. We confirmed the efficiency of MHC class I antigen presentation in DCs with/without 1 h incubation after US exposure. The efficiency following 1 h incubation was higher than that without incubation (data not shown). This result suggests that the membrane permeability of DCs increases even after US exposure. Although the mechanism behind antigen delivery by BLs is unknown, our data support a temporary increase in permeability of the plasma membrane after US exposure. Moreover, recent data from microbubble studies suggest that the resealing of US-induced pores is an energy-dependent process, with the cells exhibiting morphological features consistent with an active and vesicle-based wound-healing responses [45]. Therefore, cells treated with sonoporation are viable due to this recovery mechanism. In this study, the viability of the DCs treated with BLs and US exposure was maintained more than 85% (Fig. 3). The accumulated evidence suggests that the combination of BLs and US exposure is an unique antigen delivery system which can deliver exogenous antigens into the cytosol without serious damage to DCs.

In this study, exogenous antigens, directly delivered into the cytosol of DCs by means of BLs and US exposure, were presented on MHC class I molecules. In addition, immunization of DCs treated with antigen, BLs and US exposure effectively primed antigen-specific CTLs. On the other hand, MHC class I antigen presentation lead to low-level

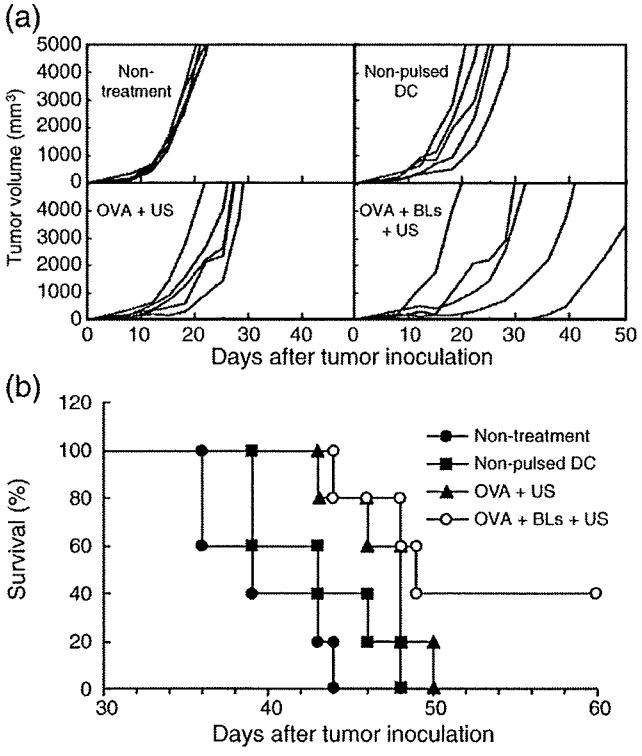

Fig. 6. Immunization of DCs treated with antigen, BLs and US exposure: therapeutic effect on tumor growth. E.G7-OVA cells were intradermally inoculated into the backs of C57BL/6 mice. On day 9, at a tumor size of 8–10 mm, OVA pulsed DCs were intradermally injected into the backs of the mice. On day 12, DCs were injected similarly. The tumor volume and survival of the mice was monitored. (a): Tumor volume of the mice after tumor inoculation. Each line indicates the tumor volume in individual mice. (b): Survival rate of the mice after tumor inoculation. All treated groups contained five mice.